Available online at www.sciencedirect.com
ScienceDirect
Physics Letters A 372 (2008) 2056–2060
PHYSICS LETTERS A
www.elsevier.com/locate/pla

Bifurcated states of the error-field-induced magnetic islands

L.-J. Zheng *, B. Li, R.D. Hazeltine

Institute for Fusion Studies, University of Texas at Austin, Austin, TX 78712, USA

Received 29 October 2007; accepted 6 November 2007

Available online 12 November 2007

Communicated by F. Porcelli

Abstract

We find that the formation of the magnetic islands due to error fields shows bifurcation when neoclassical effects are included. The bifurcation, which follows from including bootstrap current terms in a description of island growth in the presence of error fields, provides a path to avoid the island-width pole in the classical description. The theory offers possible theoretical explanations for the recent DIII-D and JT-60 experimental observations concerning confinement deterioration with increasing error field.
Published by Elsevier B.V.

PACS: 52.35.Py; 52.55.Fa; 52.55.Hc

Neoclassical tearing modes (NTMs) [1–4], resistive wall modes (RWMs) [5,6], and error-field-induced magnetic islands [7,8] are important issues for magnetic confinement of the fusion plasmas. Extensive experimental and theoretical studies have been performed to investigate them. Notably, the recent DIII-D and JT-60 tokamak experiments show that, when rotation braking is supplied by the counter neutral-beam injection rather than by error fields, the critical rotation frequency is reduced by one order of magnitude (from about 0.05 to 0.003, normalized by Alfvén frequency) [9,10]. The importance of this development lies in the fact that the new critical rotation frequency is at a level achievable in the ITER design. In addition, JT-60 experiments show that the introduction of ferritic steel tiles (FSTs) for reducing the error field raises significantly the achievable beta limit [10]. One of the theoretical explanations for this sharp change in the critical rotation frequency bifurcation is based on classical island bifurcation theory in Refs. [8] and [7]. The friction between static magnetic islands and exterior rotating plasma causes bifurcated states: the "unreconnected" state with the magnetic islands completely torn away by the rotation, and the "fully reconnected" state in which the islands survive [9]. The other explanation attributes the bifurcation to the distinct RWM stability properties, corresponding to the different rotation profiles generated by counter neutral-beam injection and error-field braking respectively [9,10].

In this Letter, we show that the formation of error-field-induced islands in the neoclassical description is intrinsically bifurcated, even in the absence of rotation. It resolves the theoretical difficulty in the conventional description, which yields an universal pole at $\Delta'_\infty = 0$ [for definition see Eq. (13)] for island width. Our theory offers a possible theoretical explanation for the confinement deterioration with error field braking in the recent DIII-D and JT-60 experiments and also may explain why JT-60 without FSTs faces a hard beta limit, not apparent in the presence of FSTs.

For simplicity a cylinder equilibrium model is employed. We use the coordinate system (r, θ, z), where r denotes the minor radius, θ represents the azimuthal angle, and z is the longitudinal coordinate. Here, the longitudinal coordinate z is related to the tokamak axisymmetric toroidal angle ϕ by $z = R\phi$, where R is the major radius. The equilibrium magnetic field is represented as $\mathbf{B} = \mathbf{B}_z + \mathbf{B}_\theta(r)$, where the longitudinal magnetic field $\mathbf{B}_z$ is constant and the poloidal magnetic field $\mathbf{B}_\theta$ is a function of r. (We use boldface to represent a vector.) The safety factor is defined as $q = rB_z/RB_\theta$.

* Corresponding author.
E-mail address: lzheng@mail.utexas.edu (L.-J. Zheng).

0375-9601/$ – see front matter Published by Elsevier B.V.
doi:10.1016/j.physleta.2007.11.017

We assume that the mode singular layer, wall, and error field current layer are thin. Then the model configuration can be described as follows. The plasma is confined in the region $r \leqslant a$, with a being the (minor) plasma radius. This plasma column is surrounded by an inner vacuum region, $a < r < b^-$, which extends to the wall. The resistive wall occupies the annular region $b^- \leqslant r < b$; immediately outside the wall, in the region $b \leqslant r \leqslant b^+$, is the error field current layer. Finally, outside the error field current layer is the outer vacuum region, $r > b^+$, which extends to infinity.

Because angular harmonics are uncoupled in cylindrical theory, it suffices to consider a single Fourier component of the perturbation: $\psi \propto \exp\{im\theta - in(\phi - \phi_0)\}$. Here, ψ is related to the radial perturbed magnetic field δB_r by $\psi = (ir/m)\delta B_r$ and ϕ_0 specifies the "O" point of the reference magnetic island. It is assumed that there is only a single resonance surface in the plasma region; the radius of this resonance is denoted by r_s, where $q(r_s) = m/n$. It is also assumed that the error-field perturbation has the same helicity as the mode. (More generally, the error field could introduce coupling between modes of different helicity; we ignore the coupled case for simplicity.)

We treat both vacuum regions as regions of vanishing plasma current and pressure. Then all regions can be described summarily by a second-order differential equation of the form [11,12]:

$$\psi'' + g_1\psi' + g_2\psi = 0, \tag{1}$$

where g_1 and g_2 depend in general on the plasma current and pressure, and the prime denotes a derivative with respect to r. Eq. (1) has two independent solutions; its general solution can be expressed as the linear summation of the two independent solutions.

Consider first the outer vacuum region, where $r > b^+$. Here the boundary condition requiring ψ to vanish at infinity eliminates one independent solution. The remaining solution can be found to be $\psi_4 = \psi_4(b^+)b^m/r^m$, where $\psi_4(b^+)$ is a constant that will be specified later. The general solution of Eq. (1) in the outer vacuum region is therefore

$$\psi(r) = c_4\psi_4(r), \tag{2}$$

where c_4 is a constant.

The region between the mode singular layer r_s and the resistive wall includes a plasma region $r_s < r \leqslant a$ as well as the inner vacuum region $a < r < b^-$. Assuming that there is no surface current flowing on the plasma-vacuum interface, we conclude that both ψ and ψ' are continuous across the plasma-vacuum interface $r = a$.

The two independent solutions in this combined region are denoted by $\psi_2(r)$ and $\psi_3(r)$. Without losing generality, we choose ψ_2 to be the solution which is continuous to ψ_4 in the outer vacuum region. Thus $\psi_2(r)$ satisfies the boundary condition

$$\psi_2\big(b^-\big) = \psi_4\big(b^+\big), \qquad \psi_2'\big(b^-\big) = \psi_4'\big(b^+\big). \tag{3}$$

Since it is not affected by the wall or the error field, ψ_2 can be physically interpreted as the "no-wall" solution. The other independent solution $\psi_3(r)$ can be constructed by imposing the following boundary conditions:

$$\psi_3\big(b^-\big) = 0, \qquad \psi_3'\big(b^-\big) = \text{const.} \tag{4}$$

Since the radial field perturbation corresponding to ψ_3 vanishes at the wall radius, $\delta B_r(b^-) = 0$, the solution $\psi_3(r)$ can be interpreted as the "perfectly conducting-wall" solution.

We determine the two constants $\psi_3'(b^-)$ and $\psi_4(b^+)$ (i.e., $\psi_2(b^-)$ according to Eq. (3)), by requiring

$$\psi_2\big(r_s^+\big) = \psi_3\big(r_s^+\big) = Br_s/m. \tag{5}$$

Here the factor B is introduced as a convenient normalization; the actual size of the field perturbation depends upon the constants c_i, which remain to be determined. The independent solutions $\psi_2(r)$ and $\psi_3(r)$ can be obtained by solving Eq. (1) numerically with boundary conditions in Eqs. (3), (4), and (5) imposed. The general solution of Eq. (1) in this combined region is therefore

$$\psi(r) = c_2\psi_2(r) + c_3\psi_3(r), \tag{6}$$

where c_2 and c_3 are constants. In the inner plasma region, $r < r_s$, requiring ψ to be finite at the magnetic axis excludes one independent solution. The other independent solution $\psi_1(r)$ satisfies $\psi \to r^m$. It can be constructed by solving Eq. (1) numerically with the boundary condition $r\psi'/\psi = m$ at a numerical infinitesimal r. Without losing generality, one can further impose that

$$\psi_1\big(r_s^-\big) = Br_s/m. \tag{7}$$

The general solution of Eq. (1) in the inner plasma region is therefore

$$\psi(r) = c_1\psi_1(r), \tag{8}$$

where c_1 is a constant.

To complete our solution we must impose the matching conditions across the three thin layers that in general carry electric current: the wall, the error-field current layer, and the mode-singular layer.

Consider the matching conditions across the mode-singular layer we assume that ψ is continuous across the singular layer—the usual constant ψ assumption. This implies

$$c_1 = c_2 + c_3, \tag{9}$$

where Eqs. (5)–(8) have been used. The other matching condition at r_s can be obtained from the usual NTM equation with the bootstrap [1,2], polarization [13], and transport induced currents included [14]:

$$\frac{\tau_R}{r_s^2}\frac{dw}{dt} = \Delta' + \epsilon^{1/2}\frac{L_q}{L_p}\beta_p\left(\frac{w}{w^2+w_d^2} - \frac{w_{\rm pol}^2}{w^3}\right), \tag{10}$$

where $\tau_R = \mu_0 r_s^2 \sigma_s$ denotes the resistive layer time, μ_0 is the vacuum permeability, σ_s is the conductivity of the singular layer, ϵ is the inversed aspect ratio, L_p and L_q represent the equilibrium scale lengths of pressure and safety factor, respectively, β_p is the poloidal plasma beta, $w_{\rm pol} = (L_q/L_p)^{1/2}\epsilon^{1/2}\rho_{\theta_i}$, $w_d = (2qL_q/k_\theta\epsilon)^{1/2}(\chi_\perp/\chi_\parallel)$, ρ_{θ_i} is the poloidal ion gyroradius, k_θ is the poloidal wave number, and $\chi_\perp$ and $\chi_\parallel$ are respectively the perpendicular and parallel thermal conductivities. The magnetic island width w is related to the normal perturbed magnetic field (proportional to c_1) by [15]

$$w = 4\sqrt{(L_q r_s B/mB_\theta)c_1}, \tag{11}$$

and

$$\Delta' = \frac{c_2\psi_2'(r_s^+) + c_3\psi_3'(r_s^+) - c_1\psi_1'(r_s^-)}{c_1}. \tag{12}$$

It is interesting to consider two limiting cases for Δ'. In the no-wall case, one has $c_3 = 0$ and therefore Eqs. (9) and (12) lead to $\Delta' \to \Delta'_\infty \equiv \psi_2'(r_s^+) - \psi_1'(r_s^-)$. In the perfectly conducting-wall case, one has $c_2 = 0$ and therefore Eqs. (9) and (12) lead to $\Delta' \to \Delta'_b \equiv \psi_3'(r_s^+) - \psi_1'(r_s^-)$. Using the definitions of no-wall Δ'_∞ and conducting-wall Δ'_b and Eq. (9), the expression for Δ' in Eq. (12) can be reduced to

$$\Delta' = \Delta'_b + \frac{c_2}{c_1}\left(\Delta'_\infty - \Delta'_b\right). \tag{13}$$

Next we consider matching across the wall and the error-field current layers. The thin wall and thin current layer assumptions imply that ψ is continuous, yielding $c_2\psi_2(b^-) + c_3\psi_3(b^-) = c_4\psi_4(b^+)$. Taking into account Eqs. (3) and (4), one has $c_2 = c_4$. The other condition can be derived from the so-called resistive wall equation [5]:

$$\frac{\tau_w}{b}\frac{\partial\psi}{\partial t} = \psi'(b) - \psi'\left(b^-\right), \tag{14}$$

where $\tau_w = \mu_0\sigma_w\, db$ is the resistive wall time, with d representing wall thickness and σ_w being the wall conductivity. According to Ampere's law, the error field current leads to a jump of ψ' as well

$$J_e\frac{ma^2B_\theta}{16L_q r_s B}\psi_3'\left(b^-\right) = \psi'\left(b^+\right) - \psi'(b), \tag{15}$$

where J_e is introduced to specify the error field strength at the given helicity. Because the relative phase of the error field and the field perturbation ψ is not fixed, the quantity J_e can have either sign. Inserting Eqs. (2)–(6) into Eqs. (14) and (15), one obtains the another matching condition across the wall and error field current layer

$$\frac{\tau_w}{b}\frac{\psi_2(b^-)}{\psi_3'(b^-)}\frac{\partial c_2}{\partial t} = c_2 - c_1 - \frac{ma^2B_\theta}{16L_q r_s B}J_e, \tag{16}$$

where Eq. (9) has been used.

In the static case one has of course $d/dt = 0$. Using Eqs. (11) and (13), Eqs. (10) and (16) in this case are reduced to

$$\Delta'_\infty w^2 + \epsilon^{1/2}\frac{L_q}{L_p}\beta_p w + \left(\Delta'_\infty - \Delta'_b\right)a^2J_e = 0. \tag{17}$$

Here, we have neglected $w_{\rm pol}$ and w_d effects, because, for typical tokamak parameters, $w_{\rm pol} \sim 2$ cm and $w_d \sim 1$ cm [4]. Eq. (17) has two solutions

$$w_\pm = \frac{-\epsilon^{1/2}(L_q/L_p)\beta_p \pm [\epsilon(L_q/L_p)^2\beta_p^2 - 4a^2\Delta'_\infty(\Delta'_\infty - \Delta'_b)J_e]^{1/2}}{2\Delta'_\infty}. \tag{18}$$

Here it is clear that bifurcation of the island width w results from the bootstrap current term; without bootstrap current, there is only single, positive definite solution. Furthermore, without bootstrap current, the island width w has a pole at $\Delta'_\infty = 0$. This pole would

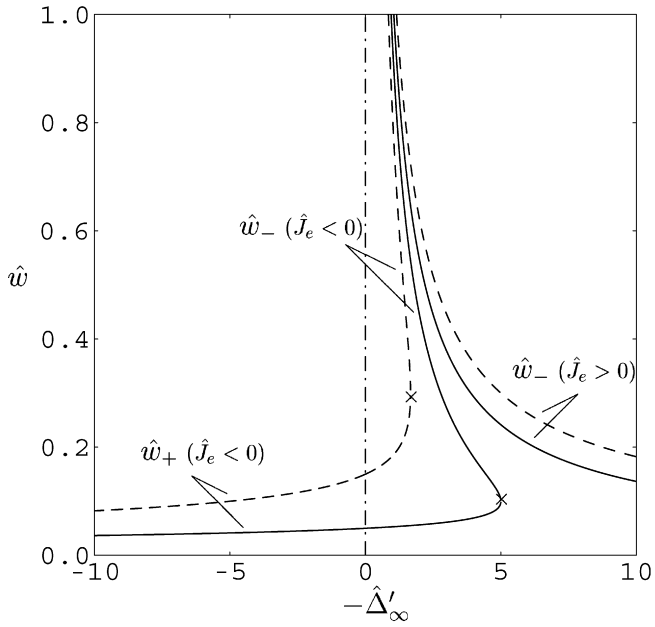

Fig. 1. Island width $\hat{w}$ versus $-\hat{\Delta}'_\infty$, with $\hat{J}_e$ as parameter. The solid curves correspond to $|\hat{J}_e| = 0.2$ and the dashed curves to $|\hat{J}_e| = 0.6$. The critical point $-\hat{\Delta}'_{\infty,c}$, which separates the ($\hat{w}_+$, $\hat{J}_e < 0$) solution and the ($\hat{w}_-$, $\hat{J}_e < 0$) solution, is marked by "×" respectively for solid and dashed curves.

imply a current or beta limit for tokamak discharges. However, as will be more apparent in the following analyses, the bootstrap current provides a path to avoid this pole, yielding island bifurcation rather than singularity.

The solutions $\hat{w}(\equiv w/a)$ in (18) are plotted in Fig. 1 versus $\hat{\Delta}'_\infty(\equiv a\Delta'_\infty/[\epsilon^{1/2}(L_q/L_p)\beta_p])$, using $\hat{J}_e(\equiv 4J_e a(\Delta'_\infty - \Delta'_b)/[\epsilon^{1/2}(L_q/L_p)\beta_p])$ as parameter. The J_e sign freedom has been tapped to get all acceptable solutions. Note also that $\Delta'_\infty - \Delta'_b$ specifies the difference of the vacuum energies with and without wall; this difference is positive in general. For 2/1 islands with $\epsilon \sim 1/5$, $\hat{\Delta}'_\infty - \hat{\Delta}'_b \sim 0.5/\hat{w}$, $L_q \sim L_p$, and $\hat{w} \approx 0.08$, one can estimate that the lower solid curve ($\hat{w}_+$, $\hat{J}_e = -0.2$) corresponds roughly to a field perturbation measured by $\delta B_r/B \sim 10^{-4}$.

Fig. 1 displays several characteristic features of the error field induced islands. First, as one can expect, a large error field gives rise to a large island: the dashed curves ($|\hat{J}_e| = 0.6$) lie always above the solid ones ($|\hat{J}_e| = 0.2$). Second, for a given error field strength $|\hat{J}_e|$, the island width is bifurcated, possessing both a large solution w_- and a small solution w_+. Third, there is a critical value of $-\hat{\Delta}'_\infty$: $-\hat{\Delta}'_{\infty,c} \equiv -1/\hat{J}_e$. Beyond the critical value, i.e., $-\hat{\Delta}'_\infty > -\hat{\Delta}'_{\infty,c}$, only the large island solution w_- exists. In Fig. 1, the critical value is denoted by "×" for two different values of $\hat{J}_e$. Note also that, as the error field $|\hat{J}_e|$ increases (making $-\hat{\Delta}'_{\infty,c}$ smaller), the island-width jump from $\hat{w}_+$ to $\hat{w}_-$ also increases, especially in the region where $-\hat{\Delta}'_\infty$ approaches its critical value.

Next we consider the DIII-D and JT-60 (with FSTs) tokamaks. The significant mode in DIII-D and JT-60 experiments is the 2/1 mode [9,10]. As computed in Ref. [12], for the 2/1 mode and typical tokamak parameters, Δ' is positive for low beta and becomes negative as beta increases. Therefore, the horizontal axis in Fig. 1 gives the direction of increasing beta for 2/1 mode. In the procedure of rotation braking by the counter neutral-beam injection, plasma rotation is braked without raising the strength of the error field. In this case error field is small. One can envisage the system evolving along the low error-field curve (lower solid line, $\hat{w}_+$) in Fig. 1, as beta ($-\hat{\Delta}'_\infty$) increases due to the heating. Since the lower solid curve features a small island width, relatively small rotation suffices to suppress island growth [7] and avoid confinement deterioration. Even when the system is heated over the critical point, $-\hat{\Delta}'_\infty > -\hat{\Delta}'_{\infty,c}$, the jump from the lower solid curve ($\hat{w}_+$) to the upper solid curve ($\hat{w}_-$, $\hat{J}_e > 0$) is still tolerable for small error field.

On the other hand, when rotation braking is accomplished by artificially increasing the error field, beta and the error field simultaneously increase. Let us also explain the confinement deterioration with large error field using Fig. 1. Initially, the plasma evolves along the low error field curve (lower solid line, $\hat{w}_+$), as beta ($-\hat{\Delta}'_\infty$) increases due to the heating. When the error field braking is applied, the system has to jump from that curve to high error field curves (dashed, $\hat{w}_-$). If the error field is applied earlier—that is, at lower values of $-\hat{\Delta}'_\infty$—than $-\hat{\Delta}'_{\infty,c}$ of high error field (i.e., of the dashed curve), the jump is from the lower solid curve ($\hat{w}+$, small $|\hat{J}_e|$) to lower dashed curve ($\hat{w}_+$, large $|\hat{J}_e|$). Continuing heating along the lower dashed curve afterward, system would face a hard beta limit at $-\hat{\Delta}'_{\infty,c}$ of high error field (i.e., of the dashed curve), since the w jump immediately ahead of $-\hat{\Delta}'_{\infty,c}$ is very big for high error field. This situation resembles to the JT-60 experiments without FSTs to be discussed later. If the error field is applied later than $-\hat{\Delta}'_{\infty,c}$ of high error field, the system would jump from the lower solid curve to the upper dashed

curve (w_-, $\hat{J}_e > 0$). Note that the high error field solutions (represented by the dashed curves) correspond to much larger island widths than the corresponding low error field solutions (represented by the solid curves).

We now turn to another interesting phenomenon: the JT-60 experiments without FSTs have been found to be difficult to drive beyond the magnetohydrodynamic limit. The present explanation attributes this limit to the insufficient neutral beam power transfer due to the ripple loss [10]. Our theory indicates that there is another fundamental reason for this hard limit. From Fig. 1, one can see that, when starting with high error field (the dashed curve labeled $\hat{w}_+$), the system beta value is limited by $-\hat{\Delta}'_{\infty,c}$. The fact that the island width jump for high error field is quite different from that for low error field may explain why the beta limit in JT-60 experiments without FSTs is much lower than that with FSTs.

In conclusion, we have shown that the formation of the error-field-induced magnetic islands is bifurcated due to the neoclassical bootstrap current. Recall that the conventional description, without neoclassical effects, yields a single solution with a pole at $\Delta'_\infty = 0$. Such an universal pole, which would impose a hard limit on beta or on plasma current regardless the strength of the error field, is not supported by experimental observation. Instead, our theory indicates that a beta or current limit in the vicinity of $\Delta'_\infty = 0$ occurs only for the large error field case. This is consistent with the finding on JT-60 that there is a hard beta limit without FSTs, while not with FSTs. The present bifurcation theory is also consistent with the DIII-D or JT-60 experimental observations that the error field braking results in a poor confinement as compared with the counter neutral-beam breaking. The rotation has not been included in the present analysis. An unified theory that includes both rotation and neoclassical effects is proposed for future studies.

References

[1] R. Carrera, R.D. Hazeltine, M. Koschenreuther, Phys. Fluids 29 (1986) 899.
[2] J.D. Callen, et al., in: Plasma Physics and Controlled Nuclear Fusion Research, vol. 2, International Atomic Energy Agency, Vienna, 1987, p. 157.
[3] Z. Chang, et al., Phys. Rev. Lett. 74 (1995) 4663.
[4] R.J. La Haye, Phys. Plasmas 13 (2006) 055501.
[5] J.P. Freidberg, Ideal Magnetohydrodynamics, Clarendon, Oxford, 1987.
[6] A.M. Garofalo, et al., Phys. Rev. Lett. 82 (1999) 3811.
[7] T.H. Jensen, et al., Phys. Fluids B 3 (1991) 1650.
[8] R. Fitzpatrick, Phys. Plasmas 5 (1998) 3325.
[9] H. Reimerdes, et al., Phys. Rev. Lett. 98 (2007) 055001.
[10] M. Takechi, et al., Phys. Rev. Lett. 98 (2007) 055002.
[11] H.P. Furth, P.H. Rutherford, H. Selberg, Phys. Fluids 16 (1973) 1054.
[12] Y. Nishimura, J.D. Callen, C.C. Hegna, Phys. Plasmas 5 (1998) 4292.
[13] F.L. Waelbroeck, et al., Phys. Rev. Lett. 87 (2001) 215003.
[14] R. Fitzpatrick, Phys. Plasmas 2 (1995) 825.
[15] P.H. Rutherford, Phys. Fluids 16 (1973) 1903.